

On the Quantum Dynamics of Thermalization

Andrew Hill

Department of Astronomy & Astrophysics
The University of Chicago, Chicago, IL 60637, USA
arhill@oddjob.uchicago.edu

1 Introduction

The importance of understanding particle thermodynamics is manifest in cosmology. The standing paradigm is to consider the thermal evolution of the distribution function, governed by the Boltzmann equations (see [1] for a review). However, this is an approximation; the full two-point Green's functions underly the true quantum thermalization process, the dynamics of which are described by the Kadanoff-Baym (KB) relations. The Boltzmann Equations (BE) are derived as approximations to these relations.

In [2], Linder & Muller numerically evolve three initial particle distributions described by a Φ^4 scalar field in unexpanding Minkowski space-time using both the KB and BE. They find KB to produce identical equilibrium thermodynamic properties for all initial conditions with fixed average energy density, while BE require the additional constraint that it be distributed over a fixed number of particles. As a result, the BE fail to accurately describe thermalization, unless the system is close to equilibrium. In particular, BE yield errant predictions for the thermodynamic temperature and chemical potential.

In this paper I derive the Kadanoff-Baym equations, discuss the approximations leading to the Boltzmann equations, review the shortcomings revealed by [2], and speculate about improvements and the cosmological impact.

2 2PI Effective Action

The dynamics of the particle distribution is determined by extreme action considerations. In the case of the real scalar field in static Minkowski space-time considered in [2], the Lagrangian density is given by

$$\mathcal{L} = -\frac{1}{2}(\partial_\mu\Phi)(\partial^\mu\Phi) - \frac{1}{2}m_B^2\Phi^2 - \frac{\lambda}{4!}\Phi^4. \quad (1)$$

We can of course construct the action from this Lagrangian by integrating over space-time. However, we are interested in the evolution of the propagator. Assuming no symmetry breaking (i.e. $\langle\Phi(x)\rangle = 0$) and Gaussian initial conditions, the action can be parameterized explicitly in the propagator as [3]

$$\Gamma[G] = \frac{i}{2}tr \log [G^{-1}] - \frac{1}{2}tr [G_0^{-1}G] + \Gamma_2[G] + const \quad (2)$$

Here the free inverse propagator is given by

$$G_0^{-1}(x, y) = (\partial_{x^\mu} \partial_{y_\mu} + m_B^2) \delta(x - y) \quad (3)$$

while the full propagator is given by the time ordered expectation value

$$G(x, y) = \langle T \{ \Phi(x) \Phi(y) \} \rangle \quad (4)$$

The factor $i\Gamma_2[G]$ relevant to equation 2 is the contribution from all two-particle irreducible (2PI) vacuum diagrams. For interacting theories this cannot be computed exactly, approximations must be made. The non-zero diagrams up to three-loop order for our Lagrangian appear in Figure 1; the resulting action is

$$\Gamma_2[G] = -\frac{\lambda}{8} \int d^4x [G(x, x) G(x, x)] + \frac{i\lambda^2}{48} \int d^4x \int d^4y [G(x, y) G(x, y) G(y, x) G(y, x)] \quad (5)$$

3 Kadanoff-Baym Equations

The equation of motion for Green's function is produced by extremizing the action. That is,

$$\frac{\delta\Gamma[G]}{\delta G(y, x)} = 0 \quad (6)$$

This can be recast as the Schwinger-Dyson equation

$$G^{-1}(x, y) = iG_0^{-1}(x, y) - \Pi(x, y) \quad (7)$$

with the proper self energy

$$\Pi(x, y) = 2i \frac{\delta\Gamma_2[G]}{\delta G(y, x)} = -\frac{i\lambda}{2} \delta(x - y) G(x, x) - \frac{\lambda^2}{6} G(x, y) G(x, y) G(y, x) \quad (8)$$

Equation 7 takes a more familiar form after substituting the expression for the free propagator given in equation 3 and convoluting with the propagator from the right

$$i(-\partial_{x^\mu} \partial_{x_\mu} + m_B^2) G(x, y) = \delta(x - y) + \int d^4z [\Pi(x, z) G(z, y)] \quad (9)$$

It is pleasing to consider the propagator as responding directly to suitably weighted properties of the field rather than having explicit δ -function dependence. To achieve this end, we note two points. First, the propagator can be separated into components

$$G(x, y) = G_F(x, y) - \frac{i}{2} \text{sign}(x^0 - y^0) G_\rho(x, y) \quad (10)$$

where the statistical propagator is

$$G_F(x, y) = \frac{1}{2} \langle [\Phi(x), \Phi(y)]_+ \rangle \quad (11)$$

and the spectral function is

$$G_\rho(x, y) = i \langle [\Phi(x), \Phi(y)]_- \rangle \quad (12)$$

Second, the self energy of equation 8 can be decomposed into a purely local and a purely nonlocal component

$$\Pi(x, y) = -i\delta(x - y) \Pi^{(local)}(x) + \Pi^{(nonlocal)}(x, y) \quad (13)$$

The local component can be considered to contribute only a mass shift and absorbed into an effective mass

$$M^2(x) = m_B^2 + \Pi^{(local)}(x) = m_B^2 + \frac{\lambda}{2} G_F(x, x) \quad (14)$$

In the fashion of the propagator, the nonlocal self energy can be separated into components. Combining equations 10 and 8

$$\Pi^{(nonlocal)}(x, y) = \Pi_F(x, y) - \frac{i}{2} \text{sign}(x^0 - y^0) \Pi_\rho(x, y) \quad (15)$$

where

$$\Pi_F(x, y) = -\frac{\lambda^2}{6} \left(G_F(x, y) G_F(x, y) G_F(x, y) - \frac{3}{4} G_\rho(x, y) G_\rho(x, y) G_F(x, y) \right) \quad (16)$$

and

$$\Pi_\rho(x, y) = -\frac{\lambda^2}{6} \left(3G_F(x, y) G_F(x, y) G_\rho(x, y) - \frac{1}{4} G_\rho(x, y) G_\rho(x, y) G_\rho(x, y) \right) \quad (17)$$

Considering these two points, equation 9 splits into the Kadanoff-Baym equations

$$(-\square_x + M^2(x)) G_F(x, y) = \int_0^{y^0} d^4z [\Pi_F(x, z) G_\rho(z, y)] - \int_0^{x^0} d^4z [\Pi_\rho(x, z) G_F(z, y)] \quad (18)$$

and

$$(-\square_x + M^2(x)) G_\rho(x, y) = - \int_{y^0}^{x^0} d^4z [\Pi_\rho(x, z) G_\rho(z, y)] \quad (19)$$

Only a single approximation was used in deriving these relations; the effective action was truncated at three loop order. By considering the equal time statistical propagator and its derivatives, the effective kinetic energy density and distribution function for a spatially homogeneous and isotropic system can be computed as [4]

$$\omega^2(t, \mathbf{p}) = \left(\frac{\partial_{x^0} \partial_{y^0} G_F(x^0, y^0, \mathbf{p})}{G_F(x^0, y^0, \mathbf{p})} \right)_{x^0=y^0=t} \quad (20)$$

and

$$f(t, \mathbf{p}) = \omega(t, \mathbf{p}) G_F(t, t, \mathbf{p}) - \frac{1}{2} \quad (21)$$

These will allow direct comparison to the results obtained for the BE.

4 Boltzmann Equations

The Boltzmann Equations are the standard tool to track the thermal evolution of the distribution function. Four approximations are necessary to derive them as approximations to the KB relations presented in §3. These result from Wigner transformation, Taylor expansion, the Kadanoff-Baym ansatz, and the quasi-particle approximation.

First we consider the Wigner transformation of equation 18. The Wigner transformation of the statistical propagator and spectral function are

$$\tilde{G}_F(t, k) = \int d^4s \exp(iks) \tilde{G}_F(t, s) \quad (22)$$

and

$$\tilde{G}_\rho(t, k) = -i \int d^4s \exp(iks) \tilde{G}_\rho(t, s) \quad (23)$$

This transformation requires the initial time be $-\infty$. Figure 2 depicts the evolution of the unequal time propagator. We see that correlations between early and late times are exponentially damped, hence we expect the negative time contributions to the integrals to be suppressed. If we also Taylor expand the effective mass and self-energy in equation 18 to first order, a quantum kinetic equation results:

$$\begin{aligned} & (2k^\mu \partial_{t^\mu} + (\partial_{t^\mu} M^2(t)) \partial_{k_\mu}) \tilde{G}_F(t, k) \\ &= \tilde{G}_F(t, k) \tilde{\Pi}_\rho(t, k) - \tilde{G}_\rho(t, k) \tilde{\Pi}_F(t, k) \\ &+ \left\{ \tilde{\Pi}_F(t, k); \Re(\tilde{G}_R(t, k)) \right\}_{PB} + \left\{ \Re(\tilde{\Pi}_R(t, k)); \tilde{G}_F(t, k) \right\}_{PB}, \end{aligned} \quad (24)$$

where the Poisson brackets are defined by

$$\left\{ \tilde{f}(t, k); \tilde{g}(t, k) \right\}_{PB} = \left[\partial_{k_\mu} \tilde{f}(t, k) \right] \left[\partial_{t^\mu} \tilde{g}(t, k) \right] - \left[\partial_{t^\mu} \tilde{f}(t, k) \right] \left[\partial_{k_\mu} \tilde{g}(t, k) \right]. \quad (25)$$

The Taylor expansion is only expected to yield good agreement when higher order derivatives are negligible. Figure 3 demonstrates this is clearly not the case for the early time statistical propagator, nor for the effective mass and self-energy since both are proportional to this quantity. We also see that after only moderate times the rapid oscillations are damped and the approximation is valid.

Next we employ the Kadanoff-Baym ansatz:

$$\tilde{G}_F(t, k) = \tilde{G}_\rho(t, k) \left(\tilde{f}(t, k) + \frac{1}{2} \right) \quad (26)$$

This is a generalization of the fluctuation dissipation theorem: the statistical propagator is proportional to the spectral function for a system in thermal equilibrium. For systems far from equilibrium this is not necessarily the case. The final approximation is the quasi-particle approximation:

$$\tilde{G}_\rho(t, k) = \frac{\pi}{E(t, \mathbf{k})} \left(\delta(k^0 - E(t, \mathbf{k})) - \delta(k^0 + E(t, \mathbf{k})) \right) \quad (27)$$

with the quasi particle energy given by

$$E(t, \mathbf{k}) = \sqrt{M^2(t) + \mathbf{k}^2} \quad (28)$$

The Poisson brackets in equation 24, corresponding to off-shell particle creation and destruction, are neglected as a result. Thus we arrive at the Boltzmann equation

$$\begin{aligned} \partial_t f(t, \mathbf{k}) = & \frac{\lambda^2 \pi}{48} \int \frac{d^3 p}{(2\pi)^3} \int \frac{d^3 q}{(2\pi)^3} \int d^3 r \left[\frac{1}{E_k E_p E_q E_r} \right. \\ & \times \delta(\mathbf{k} + \mathbf{p} - \mathbf{q} - \mathbf{r}) \delta(E_k + E_p - E_q - E_r) \\ & \left. \times \left((1 + f_{\mathbf{k}})(1 + f_{\mathbf{p}}) f_{\mathbf{q}} f_{\mathbf{r}} - f_{\mathbf{k}} f_{\mathbf{p}} (1 + f_{\mathbf{q}})(1 + f_{\mathbf{r}}) \right) \right]. \end{aligned} \quad (29)$$

5 Comparison of Numerical Results

5.1 Initial Conditions

The equations to be evolved are 18 and 19 for KB and 29 for BE. Following equation 21, the initial one-point distribution function specifies initial conditions (IC) for both sets of equations. Figure 4 depicts the three initial distribution functions considered by [2]. These particular IC have the same average energy density. The initial statistical propagator and its derivatives are:

$$G_F(x^0, y^0, \mathbf{p})_{x^0=y^0=0} = \left[\frac{f(t, \mathbf{p}) + \frac{1}{2}}{\omega(t, \mathbf{p})} \right]_{t=0}, \quad (30)$$

$$[\partial_{x^0} G_F(x^0, y^0, \mathbf{p})]_{x^0=y^0=0} = 0, \quad (31)$$

$$[\partial_{x^0} \partial_{y^0} G_F(x^0, y^0, \mathbf{p})]_{x^0=y^0=0} = \left[\omega(t, \mathbf{p}) \left(f(t, \mathbf{p}) + \frac{1}{2} \right) \right]_{t=0}, \quad (32)$$

where the initial effective energy density is given by

$$\omega(t=0, \mathbf{p}) = \sqrt{m_R^2 + \mathbf{p}^2}. \quad (33)$$

The canonical commutation relations specify the spectral function IC.

5.2 Numerical Results

Solutions of the KB and BE lead to discrepancies. Figure 5 reveals that not only do the early time behavior of the distributions differ, more importantly so do the final equilibrium values. While the KB predict the same final equilibrium value for all IC, the BE prediction differs for one IC. This point is developed in Figure 6. Again the KB predict the same final equilibrium distribution and the BE differ for a single IC. More quantitatively, the final

equilibrium distribution is Boltzmann; the inverse slope of each solution line in the Figure is the predicted equilibrium temperature, while chemical potential is proportional to the y-intercept. Unlike the KB, the BE fail to predict a vanishing chemical potential and disagree on the equilibrium temperature for one IC.

Reexamining IC3, plotted in Figure 4, it seems differ the most from thermal. Figure 7 shows that thermalization drives the distribution to favor lower momentum modes. The number density is given by the first moment of the distribution

$$n(t) = \int \frac{d^4p}{(2\pi)^3} f(t, \mathbf{p}) \quad (34)$$

As seen in Figure 8, the KB achieve this through significant particle creation and destruction. As a result of the approximations used in §4, the BE are unable to utilize this off-shell process. Since the initial number density for IC3 differs by more than numerical errors from IC1 and IC2, it remains so upon evolution by the BE.

Further differences between the KB and BE approach to thermalization of IC3 are seen in Figure 7. Even after moderate times, the KB predict a system described by a temperature and chemical potential, implying a quick approach to kinetic equilibrium. As time evolves, the temperature smoothly changes as chemical equilibrium is approached. Only at late times do the BE describe a system with temperature and (non-zero) chemical potential. Furthermore the distinct separation of timescales is absent suggesting the BE cannot distinguish between thermal and kinetic equilibrium. ‘

6 Discussion

Given different sets of IC, in general the BE predictions of the equilibrium distribution will differ, with agreement only when the ICs consist of an identical average energy density distributed over an identical number of particles. This leads to incorrect predictions for the thermodynamic temperature and chemical potential of the system. However, the KB yield the same final results only requiring the the average energy density be equal.

In situations far from chemical equilibrium, the discrepancies between KB and BE become important. Errors will be introduced when tracking the distribution with BE in this regime, such as is the case in baryogenesis [1]. Moreover, IC predicted by certain models may be incorrectly constrained unless considered with KB. Because freeze-out involves equilibrium processes, errors introduced with BE should be insignificant (although the two previous points were not considered in [2]). The application to expanding space-time and other fields and interactions would be enlightening.

References

- [1] E.W. Kolb & M.S. Turner, *The Early Universe*, Addison-Wesley (1990)

- [2] M. Linder & M.M. Muller (2005) [hep-ph/0512147]
- [3] J. Berges, **A699** (2002) 847; R. Jackiw, Phys. Rev. **D9** (1974) 1686; J.M. Cornwall, R. Jackiw, and E. Tomboulis, Phys. Rev. **D10** (1974) 2428; E. Calzetta and B.L. Hu, Phys. Rev. **D37** (1988) 2878
- [4] J. Berges, S. Borsanyi, and D.N. Voskresensky, Nucl. Phys. **A672** (2000) 313



Figure 1: Two- and three-loop contribution to $\Gamma_2[G]$. The lines represent the full connected Schwinger-Keldysh propagator.

Kadanoff-Baym

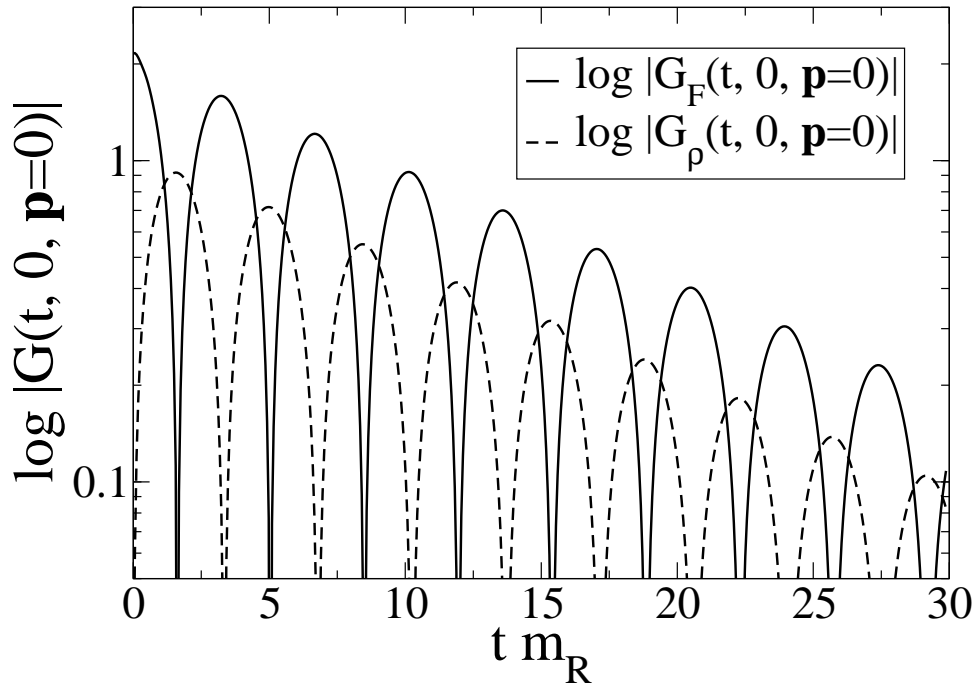


Figure 2: The time dependence of the unequal time propagator for the $\mathbf{p} = 0$ mode. The correlation between early and late times is suppressed.

Kadanoff-Baym

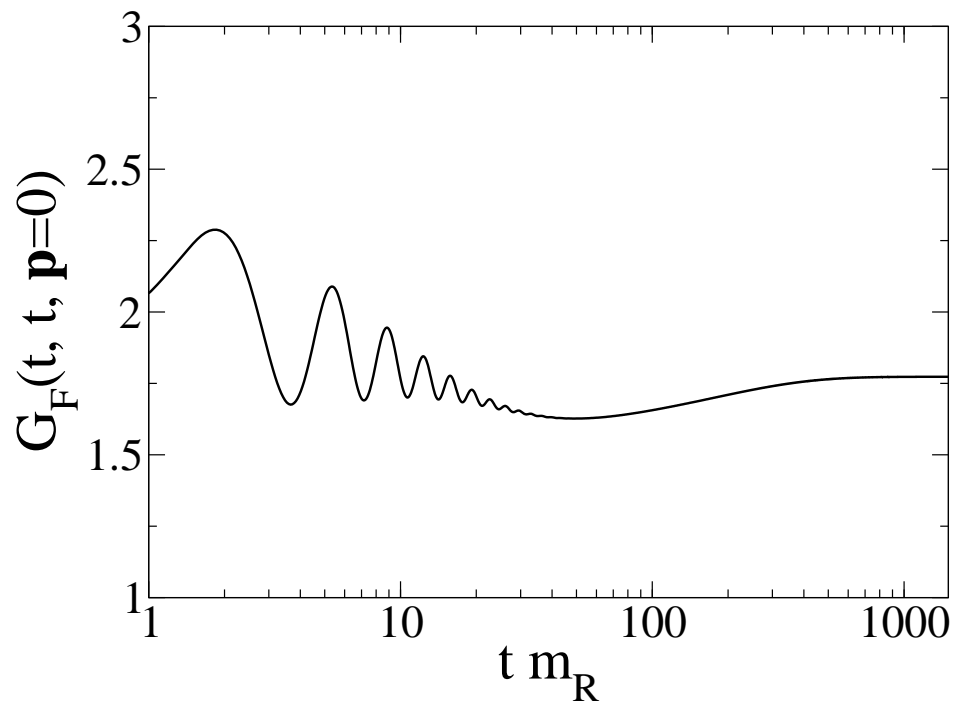


Figure 3: The time dependence of the equal time propagator for the $\mathbf{p} = 0$ mode. The rapid oscillations apparent at early times quickly decay.

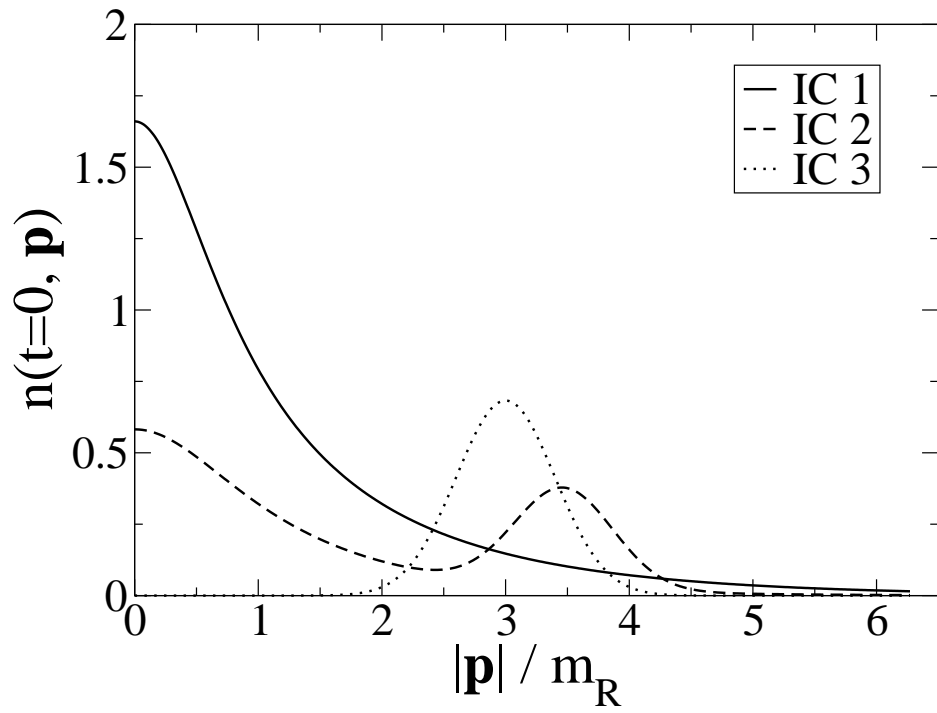
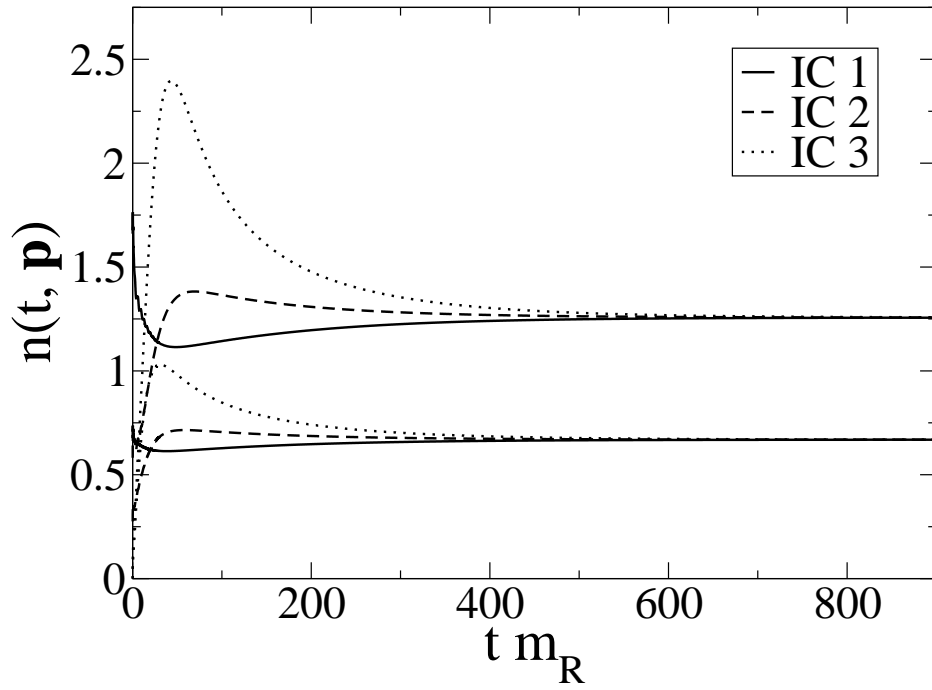


Figure 4: The initial distributions considered in [2], where the notation n is used for my f .

Kadanoff-Baym



Boltzmann

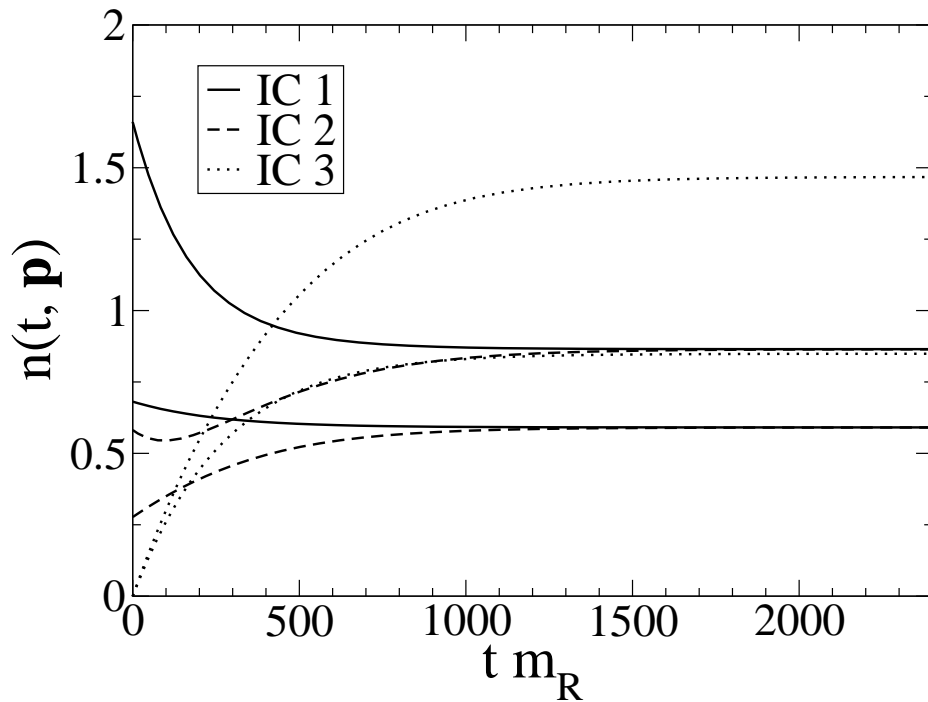
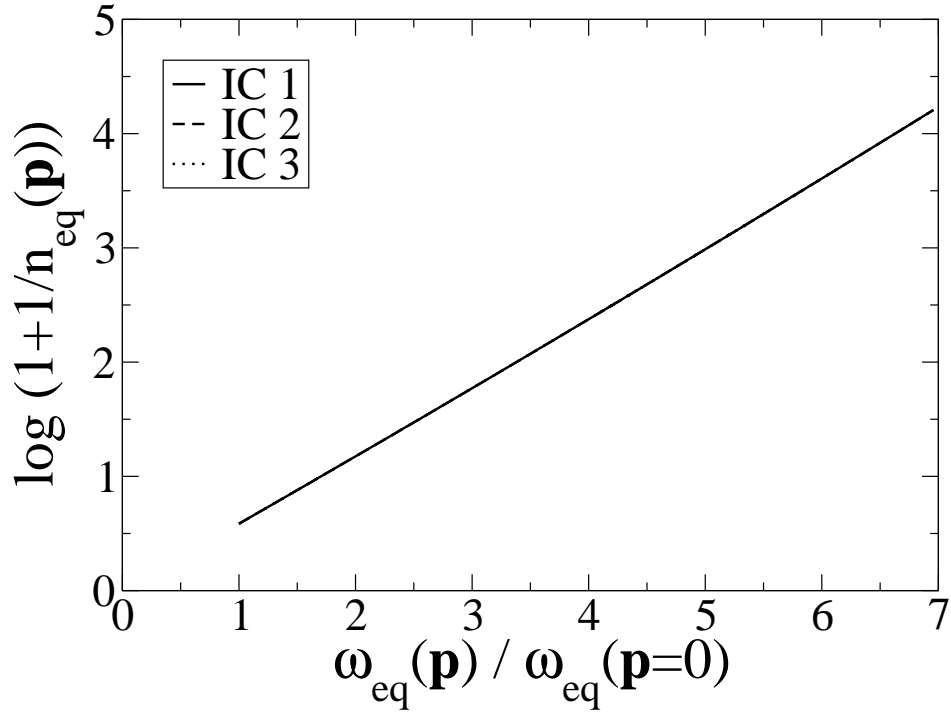


Figure 5: The time dependence of the distribution for two fixed momentum modes. Only the KB solutions evolve to the same equilibrium distribution for all IC.

Kadanoff-Baym



Boltzmann

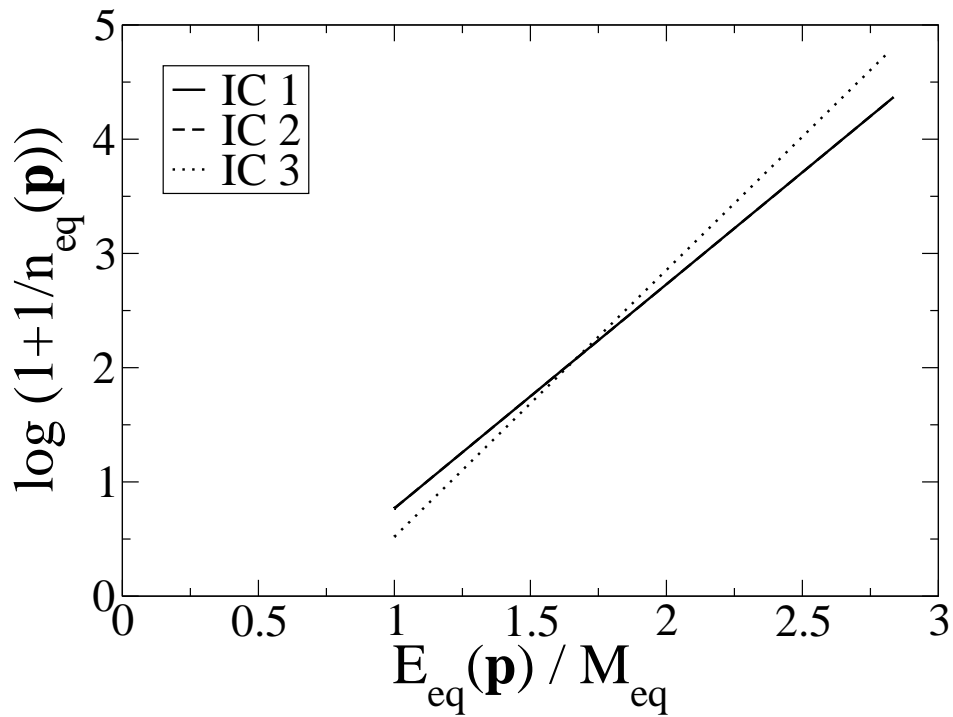


Figure 6: The equilibrium number density for each mode. Here the temperature is given by the inverse slope and the chemical potential by minus the product of the y-intercept and the slope.

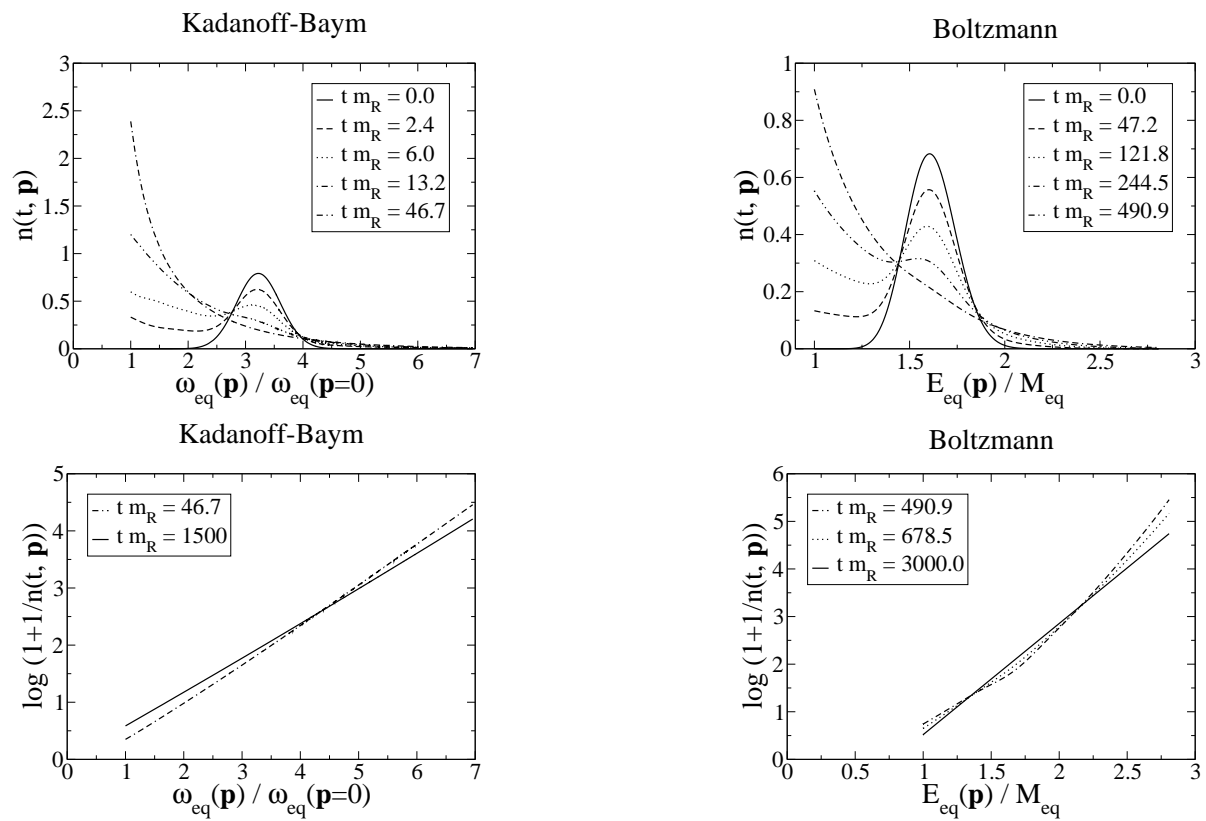
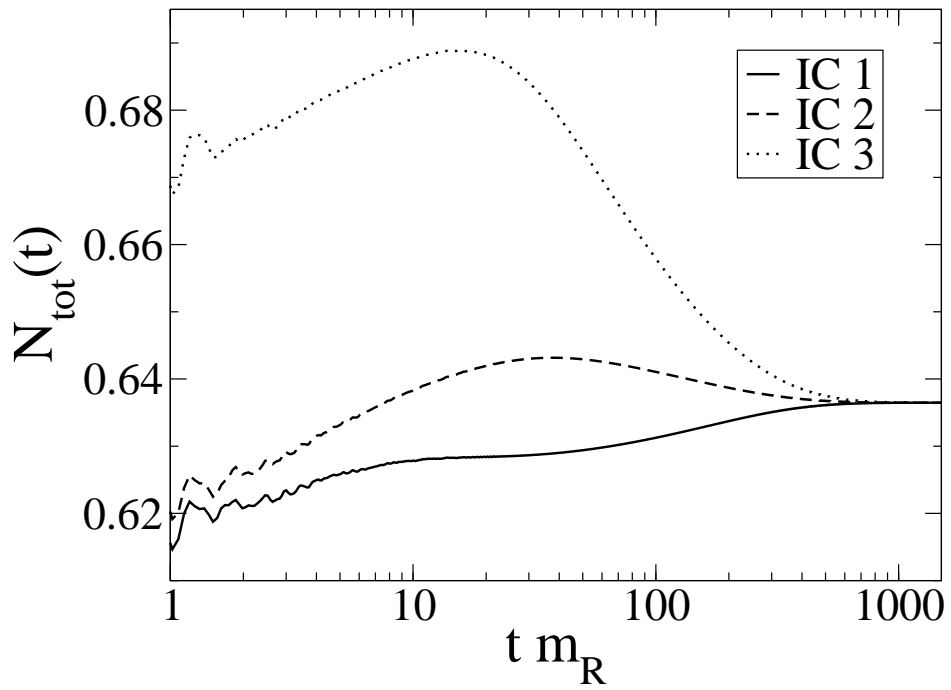


Figure 7: Evolution of IC3

Kadanoff-Baym



Boltzmann

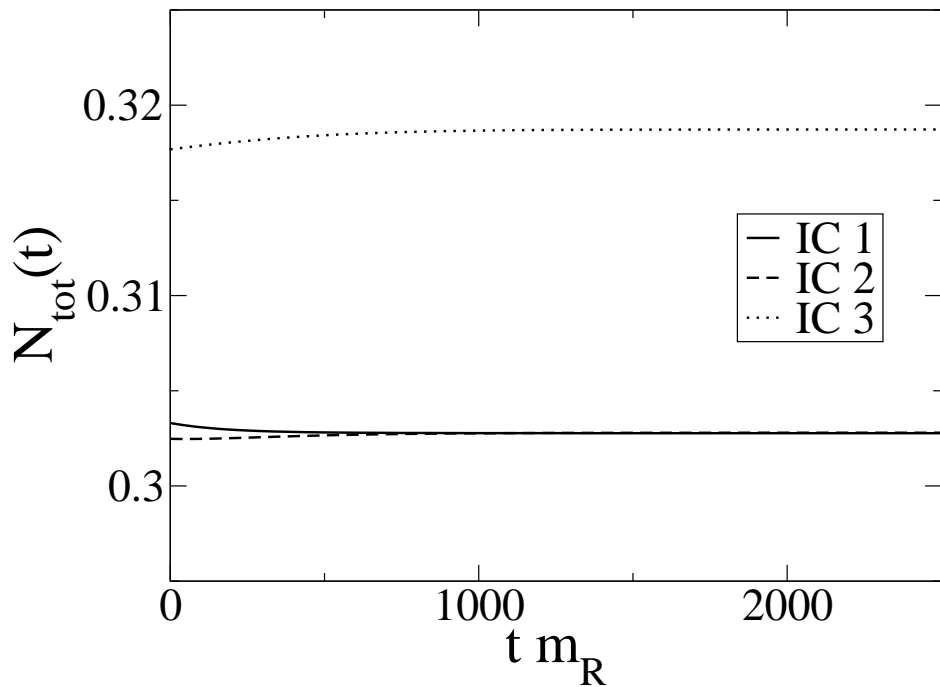


Figure 8: Evolution of number density. There is significant particle creation and destruction for the KB case, while this process is forbidden in BE.